Quantification of stable carbon and oxygen isotopic fractionation of CO_2 during photosynthesis and respiration

Geessinck S.L.[1], Karaoli A.[2], Mol E.P.[1], and Stavropoulou F.[2]

[1]Faculty of Geosciences, Department of Earth Sciences, Utrecht University
[2]Faculty of Science, Department of Physics, Utrecht University

January 2022

Abstract

In this project, the diurnal pattern of CO_2 concentration and its isotopic compositions δ^{18}O and δ^{13}C were studied during a week in October 2021. The measurements were taken in the botanical gardens in Utrecht Science Park by using a high temporal resolution (10Hz) laser trace gas monitor. The isotopic compositions were calibrated and the whole data was 10 seconds averaged before the analysis. The analysis focused on two different events when the CO_2 concentration significantly changes, one during the working week and the other during the weekend. The isotopic signatures during the increase and decrease of CO_2 of the two events were found by using the Keeling approach. For δ^{13}C, it is found that only one process took place each time, photosynthesis during the day and respiration during the night with the same δ^{13}C isotopic signature. In addition, based on literature, for both events, these values fall into the range of the δ^{13}C isotopic signature of C3 type plant respiration. However, for δ^{18}O, it is found that an average of more than one source and/or sink affected the results each time period. Therefore, the Keeling method did not work for this isotope and the identification of these processes was not straightforward. Finally, meteorological variables were used for correlation analysis to further study the variation of CO_2 concentration that is observed during the time period. The largest correlation is found between CO_2 concentration and the wind speed during the weekend. As a result, the most likely explanation for the large values of CO_2 concentration and the δ^{18}O values during the weekend is the transfer of an air plume with different characteristics coming from a different ecosystem such as Utrecht city.

1 Introduction

Carbon is one of the main greenhouse gasses and is increasing in the atmosphere. The main process that governs CO_2 are respiration and photosynthesis. The concentrations of the different stable isotopes are used to study the cycles of CO_2 through atmosphere and biosphere, since the various processes alter the relative abundances of the isotopes of carbon and oxygen.

Photosynthesis is a biochemical process in plants that produces organic matter (glucose) from stable inorganic matter under the influence of light. The overall reaction of photosynthesis can be found in the chemical reaction below [1].

$$6CO_2 + 6H_2O \xrightarrow{\text{Light}} C_6H_{12}O_6 + 6O_2 + 6O_2$$

Cellular respiration is a process that takes place in cells of organisms that convert glucose into energy (ATP) and waste products. The overall reaction of cellular respiration can be found in the chemical reaction below.

$$C_6H_{12}O_6 + 6O_2 \longrightarrow 6CO_2 + 6H_2O$$

The different stable isotopes of CO_2 are measured by their isotopic composition. The isotopic composition express the relative difference of the ratio of the molecules with heavy isotopes relative to the standard molecules. The isotopic composition is expressed through the δ notation. The delta values for ^{18}O and ^{13}C are defined, in ‰, in eqs. (1) and (2). The international standards that are used for $\delta^{18}O$ and δ^{13}C are the Vienna Standard Mean Ocean Water (VSMOW) and Vienna Pee Dee Belemnite (VPDB) respectively.

$$\delta^{18}O = \left(\frac{\left(\frac{^{18}O}{^{16}O}\right)_{sample}}{\left(\frac{^{18}O}{^{16}O}\right)_{VSMOW}} - 1 \right) \quad (1)$$

$$\delta^{13}C = \left(\frac{\left(\frac{^{13}C}{^{12}C}\right)_{sample}}{\left(\frac{^{13}C}{^{12}C}\right)_{VPDB}} - 1 \right) \quad (2)$$

1.1 δ^{13}C in atmospheric CO_2

The two main processes influencing atmospheric CO_2 concentrations and δ^{13}C values are photosynthesis and respiration. During the day, photosynthetic discrim-

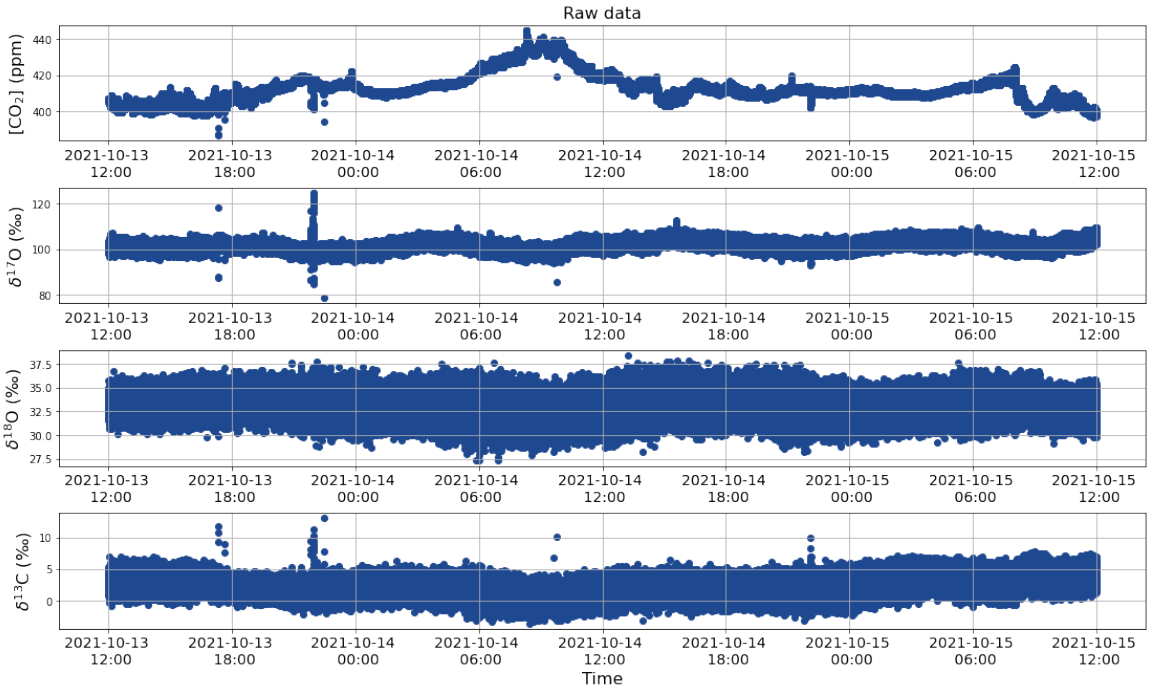

Fig. 1. Time series of the raw data of CO_2 concentration and the isotopic compositions $\delta^{17}O$, $\delta^{18}O$ and $\delta^{13}C$ during the weekdays (between 13/10/2021 12:00:10 and 15/10/2021 12:00:00)

ination dominates whereas respiration dominates at night resulting in a diurnal variation in $\delta^{13}C$ of ambient CO_2. During photosynthesis, CO_2 enters a plant by diffusing into its leaves through its stomata, where the enzyme Rubisco fixes carbon into sugar. During diffusion, fractionation occurs as plants preferentially absorb $^{12}CO_2$ instead of $^{13}CO_2$. Therefore, the air inside the plant is ^{13}C depleted, whereas the atmosphere is ^{13}C enriched. The carbon isotope composition ($\delta^{13}C$) of plants ranges from -7 to -35‰, depending on photosynthetic pathway (C3, C4 or CAM). In C3 plants, photosynthetic discrimination of carbon varies from -22 to -35‰whereas for C4 plants varies from -12 to -15‰ [2][3]. The net flux of ^{13}C between the biosphere and the atmosphere is the sum of two fluxes, the photosynthetic uptake and the respiration. CO_2 leaves the biosphere by respiration, but since all carbon is eventually respired, the $\delta^{13}C$ value is equal to the photosynthetic uptake [4].

1.2 $\delta^{18}O$ in atmospheric CO_2

The ^{18}O signal in CO_2 reflects the coupling between the global hydrological and carbon cycles. During photosynthesis, CO_2 diffuses into the leaves, readily dissolves in water and exchanges oxygen isotopes with water in chloroplasts. Water in leaves is highly enriched in ^{18}O because of the process of evapotranspiration meaning that the ^{16}O isotope evaporates faster leaving the heavy isotopes behind. In C_3 plants, about 33 % of this CO_2 is fixed in photosynthesis, the rest of the CO_2 diffuses back into the atmosphere after isotopically equilibrating with water. In other words, CO_2 that is exposed to leaf water during photosynthesis gains the isotopic signature of the leaf water which is ^{18}O enriched [5]. For C_4 plants, this enrichment is lower because the CO_2 is fixed immediately in the bundle sheet cells [6]. Therefore, the main factor on the $\delta^{18}O$ signature of CO_2 is the $\delta^{18}O$ of the liquid water with which it was last in contact.

Our purposes through this study are: a) learn to analyze and calibrate the data, b) identify the isotopic signatures using Keeling plots, c) correlate the atmospheric CO_2 with meteorological variables and d) interpret the variation of CO_2 during the days.

The paper is organized as follows: Section 2 includes information about the instrument and the data set that we used in our study as well as the data for the correlation analysis, Section 3 describes in detail the calibration of the data set, the noise reduction method applied and the Keeling plot approach, Section 4 describes the results of our analysis with all the relevant figures, and finally Section 5 closes the paper with discussion and conclusions.

2 Data and Instrument

The data set used in our study was from ambient air measurements in the botanical gardens in Utrecht Science Park over several days during a working week and over several days during the weekend. More specifically, the time period for the weekdays was from 13/10/2021 12:00:00 until 15/10/2021 12:00:00 and for the weekend was from 15/10/2021 15:30:00 until 17/10/2021 18:00:00. The instrument used was a trace gas monitor.

The instrument recorded CO_2 concentration in the

atmosphere as well as the isotopic compositions of $^{12}C^{16}O^{17}O$, $^{12}C^{16}O^{18}O$ and $^{13}C^{16}O^{16}O$. However, the determination of the $\delta^{17}O$ of CO_2 samples itself is extremely complex, due to the mass overlap of the $\delta^{13}C$ and $\delta^{17}O$ containing isotopologues, and can only be done using very advanced techniques. Therefore, the behavior of $\delta^{17}O$ will not be analyzed further.

2.1 Laser Trace Gas Monitor

The instrument used for conducting the experiments is a trace gas monitor. The principle is as following; a laser device emits light with a certain frequency ν and energy E = hν Each atom has a ground level at a specific energy (E1) and an excited level (E2). The difference of these levels is

$$E2 - E1 = \Delta E = h\nu. \tag{3}$$

The electrons in atoms can absorb the energy from the laser light if the energy difference of the levels matches the energy that is carried by the light. The adsorption of the light adds energy to the vibrational and rotational levels of the atoms, which can be measured. Because the signal detected by the detector is lower due to absorption of the light by the molecules, peaks are visible in the spectrum. An example of an infrared (IR) spectrum can be found in Fig. 2. [7]

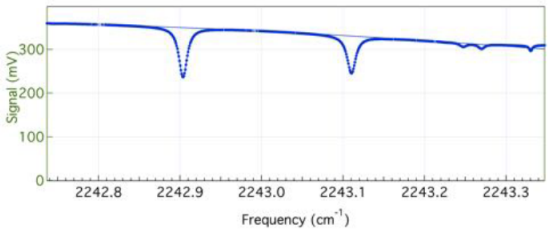

Fig. 2. An example of an infrared spectrum.

The vibrational energy of a molecule is described by

$$E_{vib} = (n+1)h\nu, \tag{4}$$

where n is a positive integer, h the planck constant and ν the vibrational frequency, that is described by

$$\nu = \frac{1}{2\pi}\sqrt{\frac{k}{\mu}}, \tag{5}$$

where k is the force constant of the bond and μ the reduced mass described by

$$\mu = \frac{m_1 m_2}{m_1 + m_2}. \tag{6}$$

The rotational energy of a molecule is described by

$$E_{rot} = \frac{h^2}{8\pi\mu r^2} J(J+1), \tag{7}$$

where J is the quantum number. The vibrational and rotational energies of eqs. (4) and (7) are both depended on the reduced mass, which is different for the different stable isotopes [8]. Because the difference in masses of the different isotopes is really small, the peaks are really close to each other. A lower pressure is required to obtain narrower peaks in the spectrum. Therefore the experiment is conducted in vacuum. The amount of light adsorbed can be translated to the number of molecules present by

$$N = A/(\alpha L), \tag{8}$$

where A is the fractional absorption, N the number density, α the absorption coefficient and L the optical path length.

2.2 Data for correlation analysis

Moreover, meteorological variables were used for correlation analysis as a further study for the changes that are observed of atmospheric CO_2 concentration. The meteorological variables used are: wind speed, global radiation and cloud cover. The data sets are downloaded from the KNMI website, from Cabauw and De Bilt's station. More specifically, the date sets provide: the mean wind speed in 0.1 m/s, the global radiation in J/cm^2 and the cloud cover in octants (9 = sky invisible). All the indices are provided as hourly time series from 01/01/2021 00:00:00 to 12/01/2022 23:00:00.

For further interpretation of the results, data sets for precipitation and wind speed are used. The precipitation is provided in 0.1 mm (-1 for $<$ 0.05 mm) while the mean wind direction in degrees during the 10-minute period (360=north, 90=east, 180=south, 270=west).

3 Methods

3.1 Noise reduction

As we mentioned in Section 2, our instrument measures data rates up to 10 Hz providing us with approximately 10 measurements per second. This results in a dataset with a huge amount of data points and a wide scatter of the values. An example of this data, is shown in Fig. 1. The noise is large enough to bury any diurnal trend and patterns of $\delta^{13}C$ and $\delta^{18}O$ are not visible. Therefore, for the interpretation of this data set, the time series need to be statistically analysed to remove the noise. This is done by calculating 10 sec averages for our data set or in other words taking the average every approximately 100 measurements. The final corrected data set used after calibration are shown in Fig. 7 and Fig. 8.

3.2 Calibration

In order to interpret the measurement results, the measured $\delta^{13}C$ and $\delta^{18}O$ values must be calibrated against an international standard (e.g. VSMOW for ^{18}O and VPDB for ^{13}C). The calibration procedure consists of two steps: firstly, there is an apparent change in $\delta^{18}O$ and $\delta^{13}C$ with changing CO_2 concentration. Furthermore, even after correcting for the effect of CO_2 concentration there is still an offset of the measurements from the real delta values.

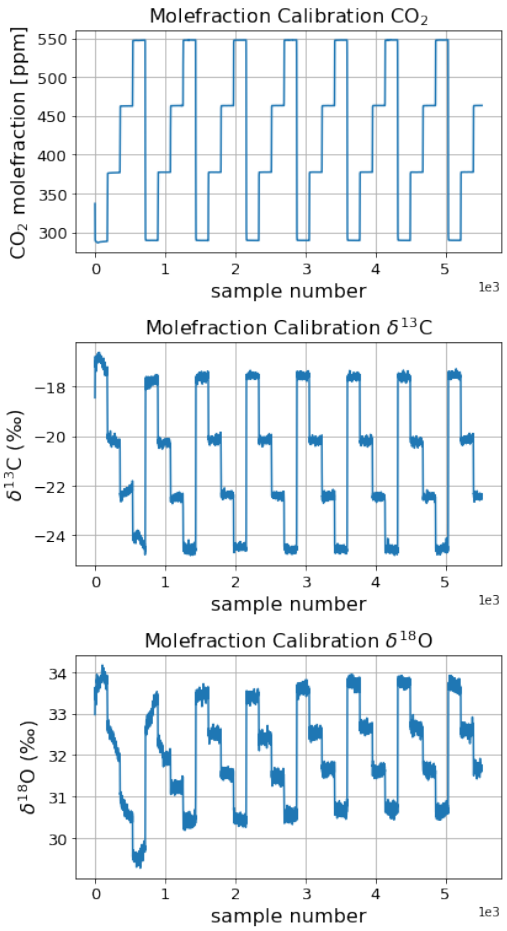

Fig. 3. CO_2, $\delta^{13}C$ and $\delta^{18}O$ measurements used for the CO_2 mole fraction calibration

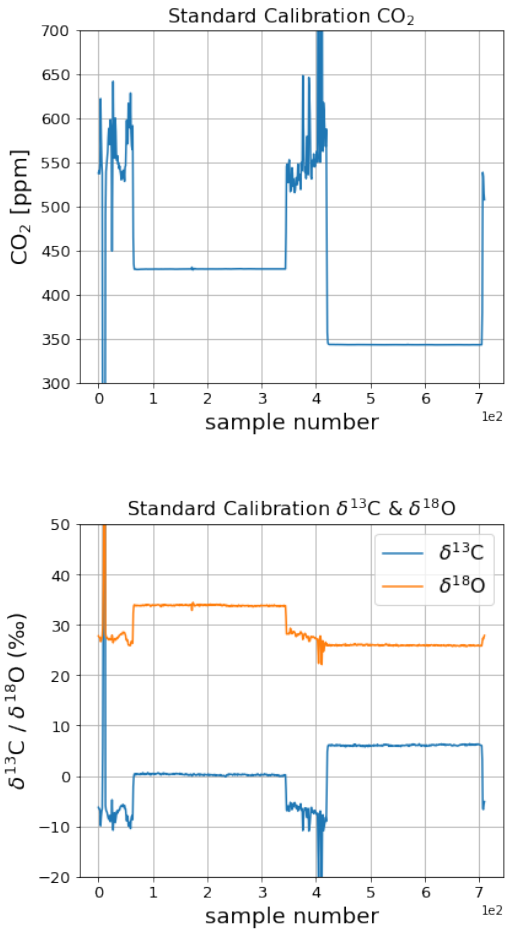

Fig. 4. Raw measurements of the CO_2 concentration, $\delta^{13}C$ and $\delta^{18}O$ of the two gas cylinders used in the calibration of raw $\delta^{13}C$ and $\delta^{18}O$ measurements to VPDB and VSMOW

In order to correct for the CO_2 concentration effect, the spectrometer was fed with different concentrations of CO_2 gas from a cylinder which had a constant (but unknown) isotopic composition. The CO_2 concentration was repeatedly increased in three steps while $\delta^{13}C$ and $\delta^{18}O$ were measured, as shown in Fig. 3. The measured $\delta^{18}O$ and $\delta^{13}C$ were then averaged for each of the CO_2 concentration steps. The three averaged $\delta^{13}C$ and $\delta^{18}O$ values were then plotted against CO_2 concentration and a second-order polynomial (ax^2+bx+c, where x is the CO_2 concentration) was fitted through the points. The mole fraction calibration curves of $\delta^{13}C$ and $\delta^{18}O$ for our measurement series are shown in Fig. 5. This calibration curve was then used to correct our measurements for the CO_2 concentration effect with respect to a reference CO_2 concentration of 400 ppm.

For the second calibration step, the $\delta^{13}C$ and $\delta^{18}O$ of two cylinders with known CO_2 concentrations and isotopic compositions were measured (Fig. 4). The measurements were first corrected for the CO_2 concentration effect with respect to a reference concentration of 400 ppm using the calibration curve derived in the first calibration step. The measured $\delta^{13}C$ and $\delta^{18}O$ values were then plotted against the real $\delta^{13}C$ (VPDB) and $\delta^{18}O$ (VSMOW) of the gas cylinders, and a calibration line was fitted through these points as shown in Fig. 6. This calibration line was used to convert our measurements to $\delta^{13}C$ and $\delta^{18}O$ with respect to the international standards.

3.3 Keeling plot

The Keeling plot analysis is an interpretation method for quantifying carbon exchange processes between terrestrial reservoirs and the atmosphere and is commonly utilized in terrestrial carbon cycle research. The basis of the Keeling plot method is conservation of mass and it is used for the identification of isotopic signature of a source which adds an amount of gas to the background atmospheric concentration of that gas [9]. In this report, the examined gas is CO_2.

The total atmospheric concentration of CO_2 (c_t) is defined in eq. (9) as the sum of the background atmospheric CO_2 concentration (c_b) and the additional CO_2 concentration produced by a source (c_s) in the ecosystem.

$$c_t = c_b + c_s \tag{9}$$

The conservation of mass is defined as:

$$(\delta^{18}O)_t\ c_t = (\delta^{18}O)_b\ c_b + (\delta^{18}O)_s\ c_s \tag{10}$$

where $\delta^{18}O$ represents the isotopic composition of each $^{16}O^{12}C^{18}O$ component.

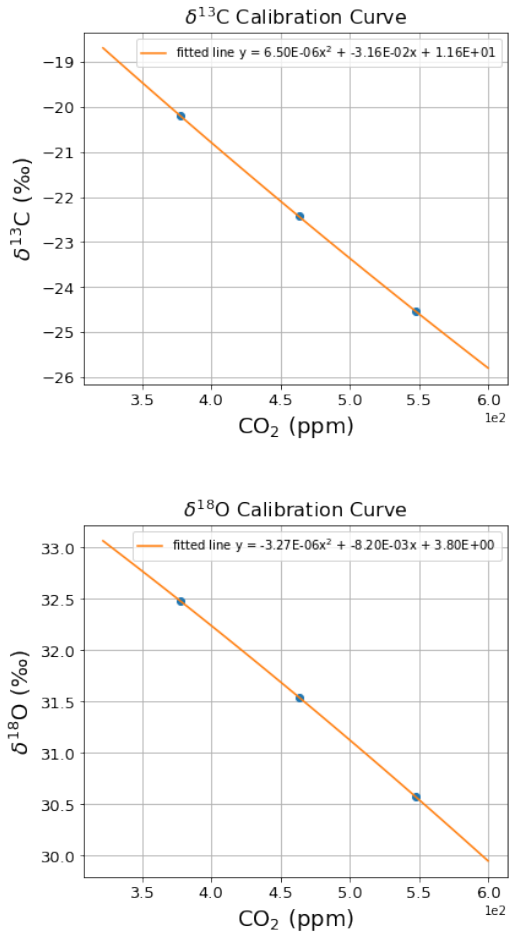

Fig. 5. Averaged $\delta^{13}C$ and $\delta^{18}O$ at the three different CO_2 concentration intervals (380, 460 and 550 ppm), and the fitted CO_2 mole fraction calibration curves for the measurement series.

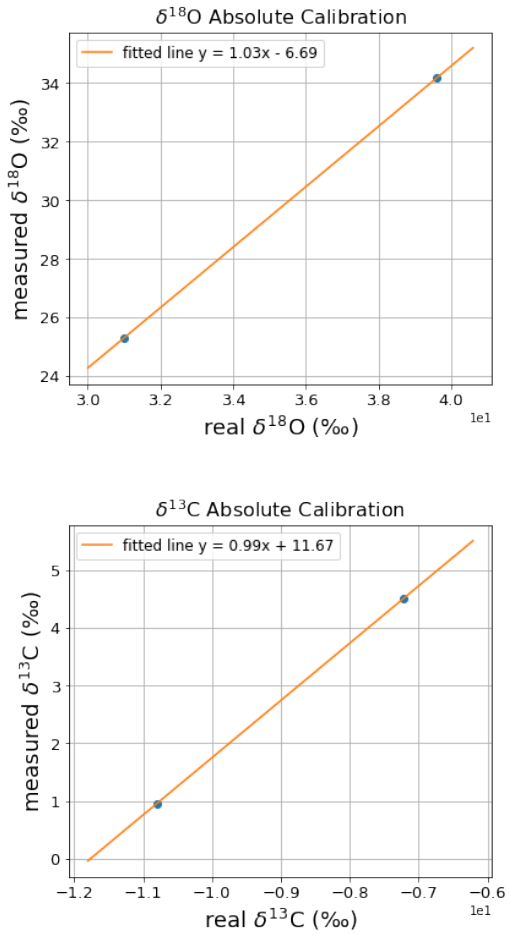

Fig. 6. Measured $\delta^{13}C$ and $\delta^{18}O$ of the CO_2 gas from two standard cylinders (corrected for CO_2 concentration with respect to a reference concentration of 400 ppm), plotted against the real $\delta^{13}C$ (VPDB) and $\delta^{18}O$ (VSMOW) of the standard cylinders. The fitted absolute calibration line is also shown.

Combining eqs. (9) and (10), we get the mathematical relationship between c_t and $\delta^{18}O_t$. [3].

$$(\delta^{18}O)_t = \frac{1}{c_t}[(\delta^{18}O)_b - (\delta^{18}O)_s] + (\delta^{18}O)_s \qquad (11)$$

Therefore, by plotting the $\delta^{18}O_t$ signature of CO_2 as a function of the inverse of the total atmospheric concentration of CO_2 (eq. (11)), we get the so-called Keeling plot. The y-intercept of the linear regression function of eq. (11) gives us the isotopic signature $\delta^{18}O_s$ of the carbon added to the reservoir (the source). Eqs. (10) and (11) can be similarly defined for the isotopic component $^{16}O^{13}C^{16}O$.

4 Results

In Figs. 7 and 8 the time series of the 10sec calibrated data of CO_2 concentration and the ^{13}C and ^{18}O isotopic compositions between 13/10 and 17/10 are illustrated. During these days, there is a large variation of both CO_2 concentration and the isotopic compositions. In this study, we focus on analyzing the data for two different events when the atmospheric CO_2 concentration significantly changes. The first event is on 14/10/2021 between 02:00 and 15:00 when the CO_2 concentrations reach values of around 440ppm. The second one is between 15/10/2021 at 16:00 and 16/10/2021 at 16:00. In this case, the CO_2 concentrations reach values of more than 500ppm. For each time period, we investigate two phases: the time period when CO_2 increases and the time period when the CO_2 decreases. For the first event, CO_2 increases from 14/10/2021 2:00 until 10:00 and then decreases from 10:00 until 15:00. For the second event, CO_2 increases from 16:00 on 15/10/2021 until 5:00 the next day, and then decreases from 5:00 on 16/10/2021 until 16:00.

For each event, the isotopic signatures of the source and the sink of the atmospheric $^{16}O^{12}C^{18}O$ and $^{16}O^{13}C^{16}O$ are computed using the Keeling plot analysis. The Keeling plots for each isotope molecule of CO_2 for the first and the second event are shown in Fig. 9 and Fig. 10 respectively.

By looking the Keeling plot of $\delta^{18}O$ for the second event in Fig. 10 (a), the expected linear relationship between the variables is not visible. We hypothesize that more than one processes contribute to the variation of $^{16}O^{12}C^{18}O$ in the air. As can be seen in the plot, the data points seem to be split into one part in

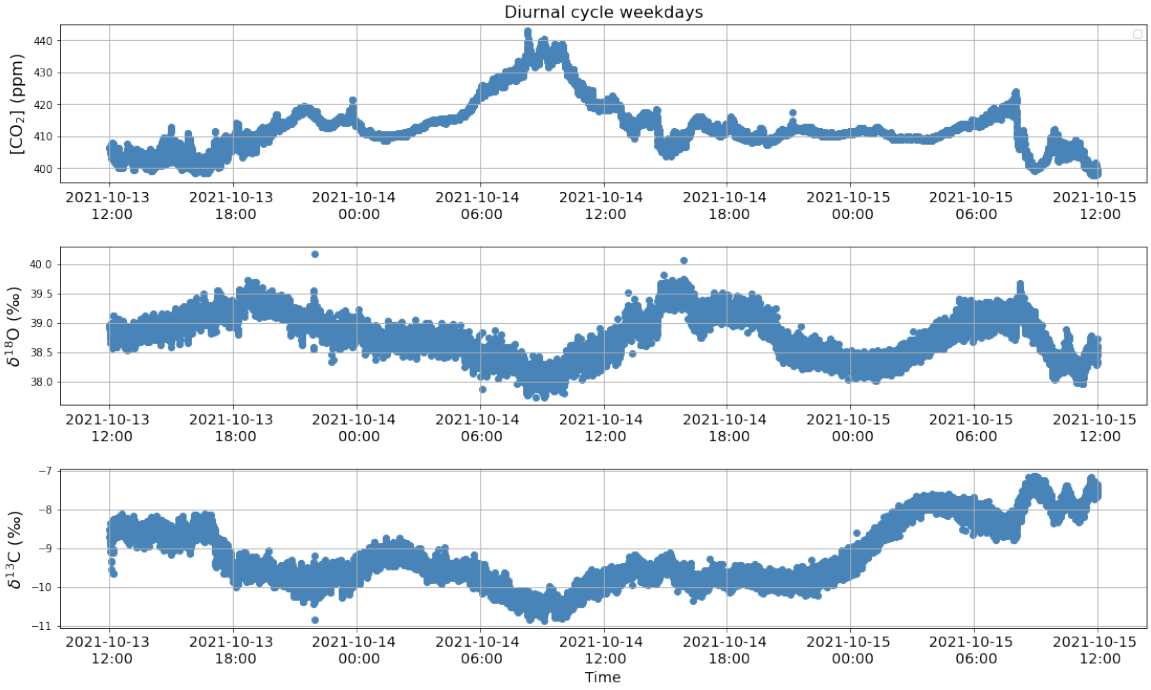

Fig. 7. Time series of the 10s averaged calibrated data of CO_2 concentration and the isotopic compositions, $\delta^{18}O$ and $\delta^{13}C$, during the weekdays (between 13/10/2021 12:00:10 and 15/10/2021 12:00:00)

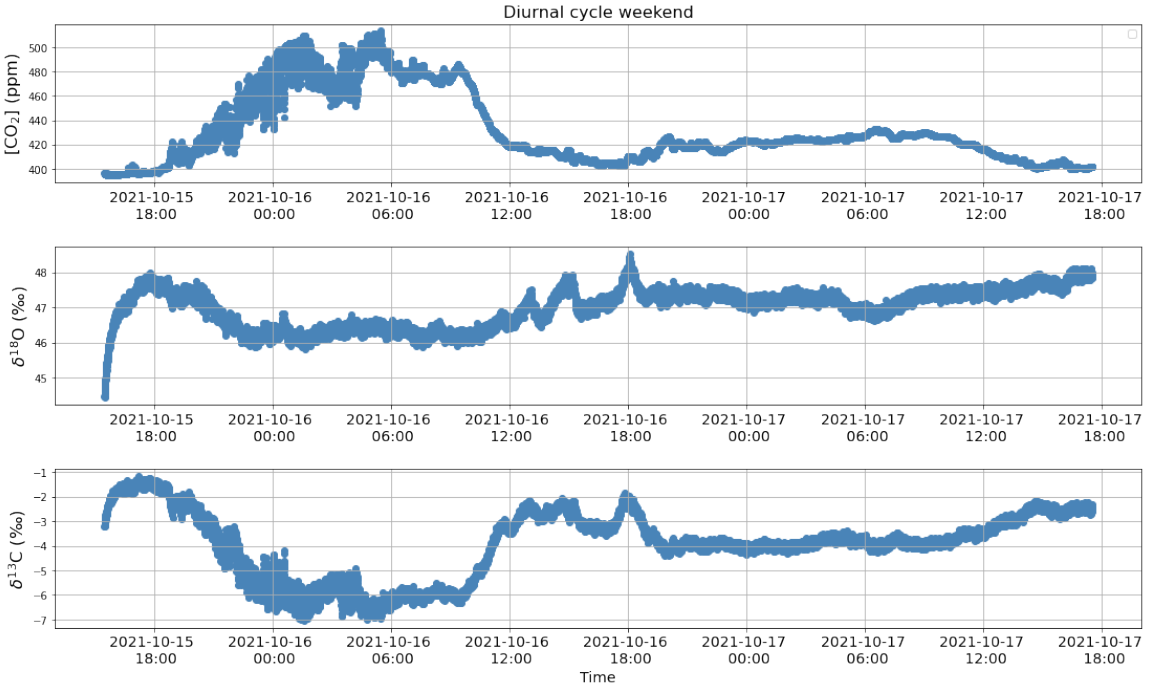

Fig. 8. Time series of the 10s averaged calibrated data of CO_2 concentration and the isotopic compositions, $\delta^{18}O$ and $\delta^{13}C$, during the weekend (between 15/10/2021 15:30:50 and 17/10/2021 17:30:00)

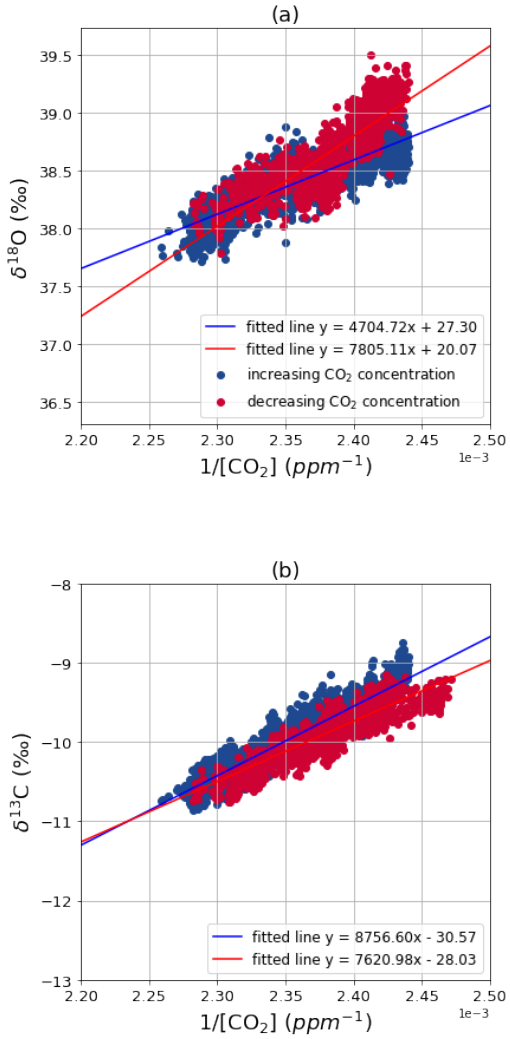

Fig. 9. Keeling plots for $\delta^{18}O$ (a) and $\delta^{13}C$ (b) during the first event (weekday). The blue points correspond to the data points during the time period that the CO_2 concentration increases and the blue line represents the fitted line of this data. The red points correspond to the data points during the time period that the CO_2 concentration decreases and the red line represents the fitted line of this data.

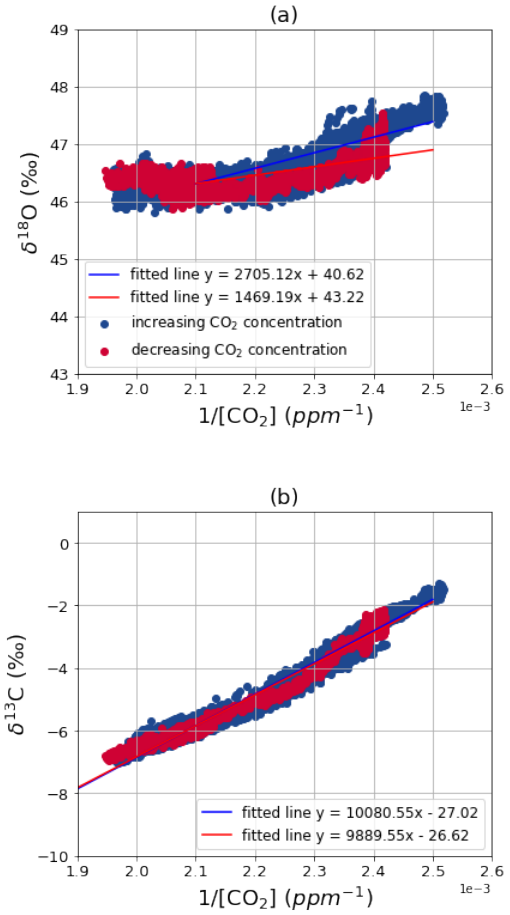

Fig. 10. Keeling plots for $\delta^{18}O$ (a) and $\delta^{13}C$ (b) during the second event (weekend). The blue points correspond to the data points during the time period that the CO_2 concentration increases and the blue line represents the fitted line of this data. The red points correspond to the data points during the time period that the CO_2 concentration decreases and the red line represents the fitted line of this data.

which the $\delta^{18}O$ remains relatively constant and a second part in which there is a more of a linear increase in the values. Therefore, we split the data sets into two smaller data sets as depicted with different colors in Fig. 11. In this way, we can identify more than one isotopic signature of $\delta^{18}O$ during the second event. All the results are shown in Tab. 1.

Finally, according to correlation analysis, although a correlation between the global radiation and CO_2 variation was found, we assume that this correlation is invalid. This is because the cloud coverage during these days was 8 octants which corresponds to a completely cloudy sky and as a result, much less radiation reaches the land. Therefore, CO_2 concentration cannot be affected by the solar incoming radiation. In addition, CO_2 variation and cloud cover cannot be correlated because the latter was constant during both events. Furthermore, the correlation value between CO_2 concentration and the wind speed is found -0.20 for the first event and -0.81 for the second event.

5 Discussion and Conclusions

By looking at the time series of CO_2 and the isotopic compositions $\delta^{13}C$ and $\delta^{18}O$ in Figs. 7 and 8, we observe that while the concentration of atmospheric CO_2 increases, both isotopic compositions decrease and vice verca. During the day when photosynthetic rates are high, ecosystems absorb atmospheric CO_2 whereas during the night ecosystem fluxes are dominated by respiration, and atmospheric CO_2 concentrations slightly increase. Since plants preferentially use $^{12}CO_2$ in photosynthesis, the CO_2 left behind in the atmosphere is enriched in $^{13}CO_2$ resulting in higher $\delta^{13}C$ (less negative) values during the day. Similarly, once inside the leaf, oxygen in water can exchange readily with oxygen in CO_2. This results in the diffusion of a ^{18}O enriched CO_2 back to the atmosphere, thus in enrichment of ^{18}O in the atmosphere during the day and reduction during the night. Notice that this is not the case for the sec-

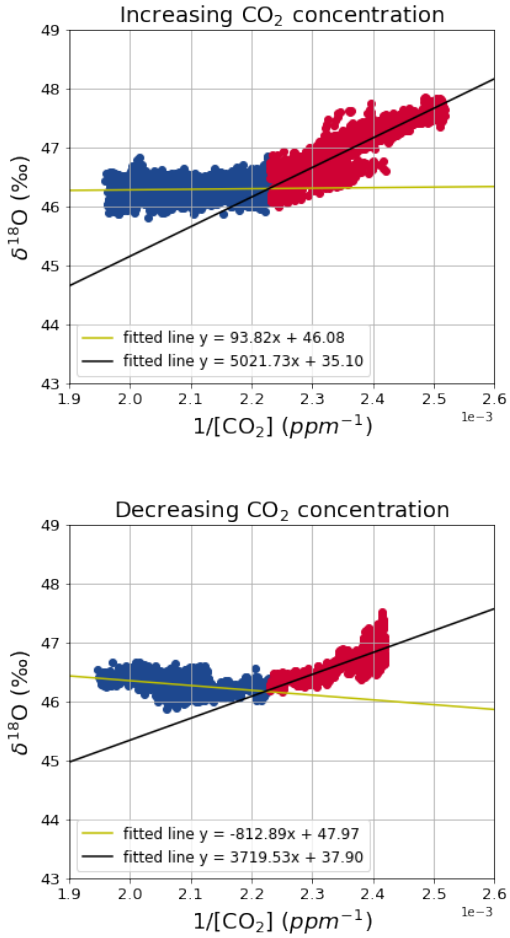

Fig. 11. The upper Keeling plot shows the data points during the time period that the CO_2 concentration increases and the lower plot shows the data points during the time period that the CO_2 concentration decreases. In both cases, the data is split in smaller data sets (blue and red data points).The black and the yellow lines represent the fitted line for each smaller data set.

ond event that we analysed on the 15/10-16/10. The CO_2 and $\delta^{13}C$ values are anti correlated as expected but the $\delta^{18}O$ values almost remain constant for most of the night. Even though there is a small reduction in the $\delta^{18}O$ when CO_2 starts increasing, the stability of the values after this small decrease governs this time period.

Another reason for this diurnal pattern could be the fact that terrestrial exchange of carbon and oxygen isotopes with the atmosphere is correlated diurnally with the Planetary Boundary Layer (PBL) dynamics. During the night, when stable air conditions are present, a shallow Nocturnal Boundary Layer (NBL) is formed. This NBL traps the respired CO_2 with depleted $\delta^{13}C$ or $\delta^{18}O$ near the surface resulting in a large decline in $\delta^{13}C$ or $\delta^{18}O$ right before sunrise. However, with the onset of photosynthesis in the morning when the sun starts shining and mixing starts happening, there is a breakdown of the PBL and $\delta^{13}C$ and $\delta^{18}O$ start increasing again. Additionally, the PBL's properties such as strength and thickness, have a considerable influence on the diurnal variability of the isotopes. Depending on the intensity of radiative cooling and subsidence, cloud cover and change in potential temperature across the entrainment zone, there can be a strong inversion in a shallow layer with a substantial nighttime decrease in $\delta^{13}C$, or a weak inversion in a deep layer with a moderate nighttime decrease in $\delta^{13}C$ [10]. The influence of the PBL could also explain the reason why, for the first event, the CO_2 values reach a peak at around 9-10 am which is later in the morning than when the sun starts rising and respiration gives way to photosynthesis.

From the Keeling plots in Fig. 9 and Fig. 10, we can identify the carbon isotopic signature of the source and the sink for the two different events. For both plots, the linear fitting works quite well, in particular for the second event. For the first event, the y-intercepts of the fitting lines for the increasing and decreasing CO_2 concentration parts are -30.57 ± 0.12‰ and -28.03 ± 0.21‰ respectively. For the second event, we get values of -27.02 ± 0.062‰ and -26.62 ± 0.057‰ for the increasing and decreasing parts respectively. For both events, the $\delta^{13}C$ isotopic signature of the process causing the increase of CO_2, so the source, is very similar to the $\delta^{13}C$ isotopic signature of the sink. However, the uncertainties calculated might indicate otherwise since the values do not fall into the errors range. On the other hand, by looking at the graphs, the data agrees pretty well and therefore, we believe that the uncertainties are underestimated. Additionally, photosynthetic and respiratory isotope effects on the atmosphere are in many cases approximately equal [3]. Thus, we can assume that there is only one process affecting our results during the night time and this is respiration whereas during the day photosynthesis replaces respiration with the same $\delta^{13}C$ isotopic signature. With reference to photosynthetic pathways, there is a large difference between the isotopic signatures of C3 plants and C4 plants as we mentioned in the introduction section. Therefore, based on literature, for both events, these values fall into the range of the $\delta^{13}C$ isotopic signature of C3 type plant respiration [11].

For the Keeling plots of ^{18}O, we find that the Keeling approach does not work as well as for the ^{13}C, as we already mentioned in Section 4 of the results. In the second and highest concentration event (Fig. 11), by splitting the data points into two different data sets and analysing them separately, we find that there is not one constant source affecting the $\delta^{18}O$ but possibly two sources; one with $\delta^{18}O$ value of between +46‰ and +48‰ and another one with $\delta^{18}O$ value of between +35‰ and +38‰. Similarly, by looking at the resulting y-intercept values of Fig. 9 for the first event, we find that there are again two processes influencing our results. One process causing the increase of CO_2 concentration with an ^{18}O isotopic composition of $+27.3 \pm 0.11$‰ and another process causing the decrease of CO_2 later in the day with an ^{18}O isotopic composition of $+20.07 \pm 0.26$‰. The $\delta^{18}O$ signature of CO_2 is primarily influenced by the $\delta^{18}O$ of the liquid water with which it was most recently in contact. Thus, a first possible hypothesis for the ^{18}O values we find, would be the influence of a precipitation event.

Isotopic composition	First event		Second event	
	increase	decrease	increase	decrease
δ^{13}C (‰)	-30.57 ± 0.12	-28.03 ± 0.21	-27.02 ± 0.062	-26.62 ± 0.057
δ^{18}O (‰)	27.30 ± 0.11	20.07 ± 0.26	46.08 ± 0.1	47.97 ± 0.12
			35.10 ± 0.15	37.90 ± 0.26

Tab. 1. Isotopic signatures δ^{13}C and δ^{18}O for the two events (unitls in ‰).

However, this hypothesis was rejected since there was no precipitation at all during the time of the measurements.

Furthermore, for the large difference of the CO_2 values between the first and the second event, one possible hypothesis was that during the weekend or otherwise during the second event, the sky was cloudier compared to the previous weekdays and as a result the photosynthesis process is not intense as usual. So, the concentration of CO_2 increases during the day. However, CO_2 variation and cloud cover cannot be correlated because the latter was constant during both events. Therefore, the presence of this large peak is not due to the reduce of the photosynthesis process.

Advection of air masses that have passed over other ecosystems like marine, urban or industrial will influence the Keeling mixing line [3]. Therefore, another likely hypothesis for both the strong increase of CO_2 concentrations and the δ^{18}O values, would be the influence of a plume coming from a different ecosystem with a different isotopic composition during the measurement period. So, maybe due to strong winds, air masses with high concentration of CO_2 and different oxygen isotopic composition passed over the botanic garden. The correlation among the CO_2 and the wind speed gave us a small value (-0.20) for the first event and a large value (-0.81) for the second event. During the first event the wind speed was stable, so this high peak does not depend on the wind speed. In contrast, during the night of the second event, the wind speed started increasing significantly heading southwest of Cabauw station resulting to the increase of the CO_2. However, since all the indices for the meteorological variables are provided as hourly time series and not 10sec averaged values as our data set, the correlation analysis was not precise enough. Nevertheless, a possible explanation for the large values of CO_2 concentration and the δ^{18}O values during the second event is the transfer of an air plume coming from the city.

Our analysis and results demonstrate that in our study the Keeling plot approach works well for δ^{13}C but not for δ^{18}O. Even though Keeling plots are widely used for identifying the isotopic signature of a source or a sink, which alters the content of a specific gas in a reservoir, their application is based on some fundamental assumptions which limit the use of this approach. One of them is that the system consists of only two reservoirs (background and one source) and another is that during the measurement time, the isotopic ratio of the carbon or the oxygen of the source does not change [12]. For δ^{18}O, both assumptions seem not to be fulfilled. The values that we calculated based on the Keeling approach of the ^{18}O did not represent the isotopic signature of a single constant source but rather the average of more than one source and/or sink. There are dynamic effects like the PBL or advection of air masses, as well as environmental factors such as light, temperature and water availability in soil and the leaf of the plant, which affect the magnitude δ^{18}O and δ^{13}C. Finally, as we mentioned before, our errors are largely underestimated. Applying different linear regression on the data as well as not allowing for errors in x values will yield different values for the slope and the intercept. Estimating the correct uncertainty of the y-intercept of the Keeling plot is an significant part of the curve-fitting process [9]. Therefore, to better understand all the processes influencing the CO_2 and the oxygen and carbon isotopes, much more information and additional input is needed to fully explain which are the processes involved and generally explain the observed atmospheric isotope patterns.

References

[1] E.I. Rabinowitch. *Photosynthesis and related processes*. Interscience publishers, inc, New York., 1945.

[2] Biogeosphere-Atmosphere Stable Isotope Network (BASIN). *How are isotopes affected by plant processes?* URL: http://basin.yolasite.com/photosynthesis.php. [Online; accessed 29-January-2022].

[3] DE Pataki et al. "The application and interpretation of Keeling plots in terrestrial carbon cycle research". In: *Global biogeochemical cycles* 17.1 (2003).

[4] Philippe Ciais et al. "Partitioning of ocean and land uptake of CO2 as inferred by δ13C measurements from the NOAA Climate Monitoring and Diagnostics Laboratory Global Air Sampling Network". In: *Journal of Geophysical Research: Atmospheres* 100.D3 (1995), pp. 5051–5070.

[5] Pieter P Tans. "Oxygen isotopic equilibrium between carbon dioxide and water in soils". In: *Tellus B* 50.2 (1998), pp. 163–178.

[6] Affek H.P. and Yakir D. "The Stable Isotopic Composition of Atmospheric CO_2". In: *Treatise on geochemistry* 1–16.2 (2014), pp. 179–212.

[7] Aerodyne Research Inc. *Aerodyne Research Trace Gas Monitors*. 2021.

[8] Polerecky, L. *Stable isotopes in Earth Sciences (GEO4-1443), Lecture Notes - Theory behind equilibrium isotope fractionation.* 2021.

[9] John B Miller and Pieter P Tans. "Calculating isotopic fractionation from atmospheric measurements at various scales". In: *Tellus B: Chemical and Physical Meteorology* 55.2 (2003), pp. 207–214.

[10] Tans P.P. Chen B. Chen J.M. and Huang L. "Simulating dynamics of–13C of CO_2 in the planetary boundary layer over a boreal forest region: covariation between surface fluxes and atmospheric mixing." In: *Tellus B: Chemical and Physical Meteorology* 58.5 (2006), pp. 537–549.

[11] Zhu B. and Cheng W. "13 C isotope fractionation during rhizosphere respiration of C 3 and C 4 plants". In: *Plant and Soil* 342.1 (2011), pp. 277–287.

[12] Schmitt J. Köhler P. Fischer H. and Munhoven G. "On the application and interpretation of Keeling plots in paleo climate research–deciphering $\delta^{13}C$ of atmospheric CO_2 measured in ice cores." In: *Biogeosciences* 3.4 (2006), pp. 539–556.